HHS Public Access

Author manuscript

Clin Cancer Res. Author manuscript; available in PMC 2021 September 01.

Published in final edited form as:

Clin Cancer Res. 2021 March 01; 27(5): 1476–1490. doi:10.1158/1078-0432.CCR-20-2860.

Combined Inhibition of $G\alpha_q$ and MEK Enhances Therapeutic Efficacy in Uveal Melanoma.

Tyler D. Hitchman[1,2], **Gabriella Bayshtok**[1,†], **Emilie Ceraudo**[3,†], **Amanda R. Moore**[1,4,5], **Cindy Lee**[1], **Ruobing Jia**[1,6], **Naitao Wang**[1], **Mohini R. Pachai**[1], **Alexander N. Shoushtari**[7,8], **Jasmine H. Francis**[9], **Youxin Guan**[1], **Juliet Chen**[1], **Matthew T. Chang**[1,10,11,12], **Barry S. Taylor**[1,10,13], **Thomas P. Sakmar**[3,14], **Thomas Huber**[3], **Ping Chi**[1,2,4,7,8,*], **Yu Chen**[1,2,4,7,8,*]

[1]Human Oncology and Pathogenesis Program, Memorial Sloan Kettering Cancer Center, New York, NY, USA

[2]Louis V. Gerstner Jr. Graduate School of Biomedical Sciences, Memorial Sloan Kettering Cancer Center, New York, NY, USA

[3]Laboratory of Chemical Biology and Signal Transduction, The Rockefeller University, New York, NY, USA.

[4]Weill Cornell Graduate School of Medical Sciences, Cornell University, New York, NY, USA

[5]Current address: Department of Discovery Oncology, Genentech Inc, South San Francisco, CA, USA.

[6]Department of Ophthalmology, Ninth People's Hospital, Shanghai Jiao Tong University, School of Medicine, Shanghai, People's Republic of China

[7]Department of Medicine, Memorial Sloan Kettering Cancer Center, New York, NY, USA

[8]Department of Medicine, Weill Cornell Medical College, 1300 York Avenue, New York, NY, USA

[9]Opthalmic Oncology Service, Memorial Sloan Kettering Cancer Center, New York, NY, USA

[*]**Corresponding Authors:** Ping Chi, MD, PhD, Memorial Sloan Kettering Cancer Center, 1275 York Avenue, New York, NY 10065, chip@mskcc.org, Yu Chen, MD, PhD, Memorial Sloan Kettering Cancer Center, 1275 York Avenue, New York, NY 10065, cheny1@mskcc.org.

[†]These authors contributed equally to this work

Authors' Contributions

Conception and design: T.D. Hitchman, Y. Chen, P. Chi, T.P. Sakmar, E. Ceraudo, T. Huber

Development of methodology: T.D. Hitchman, E. Ceraudo, A.R. Moore, Y. Guan, J. Chen, C. Lee, G. Bayshtok, N. Wang, M. Pachai, R. Jia

Acquisition of data (provided animals, acquired and managed patients, provided facilities, etc.): Y. Chen, P. Chi, T.P. Sakmar, A. Shoushtari, J.H. Francis, B.S. Taylor

Analysis and interpretation of data (e.g., statistical analysis, biostatistics, computational analysis): Y. Chen, T.D. Hitchman, M.T. Chang, B.S. Taylor

Writing, review, and/or revision of the manuscript: T.D. Hitchman, Y. Chen, P. Chi, T.P. Sakmar, A.R. Moore, G. Bayshtok

Administrative, technical, or material support (i.e., reporting or organizing data, constructing databases): T.D. Hitchman, Y. Chen

Study supervision: Y. Chen

Disclosure of Potential Conflicts of Interest

B.S.T. reports receiving honoraria and research funding from Genentech and advisory board activities for Boehringer Ingelheim and Loxo Oncology, a wholly owned subsidiary of Eli Lilly. A. R. Moore is a postdoctoral fellow employed by Genentech/Roche. M.T. Chang is an employee of Genentech/Roche. Y Chen owns stock in ORIC pharmaceuticals.

[10]Department of Epidemiology and Biostatistics, Memorial Sloan Kettering Cancer Center, New York, New York, USA.

[11]Department of Bioengineering and Therapeutic Sciences, University of California, San Francisco, San Francisco, California, USA

[12]Current address: Department of Bioinformatics, Genentech Inc, South San Francisco, CA, USA.

[13]Marie-Josée and Henry R. Kravis Center for Molecular Oncology, Memorial Sloan Kettering Cancer Center, New York, New York, USA.

[14]Division of Neurogeriatrics, Department of Neurobiology, Care Sciences and Society, Karolinska Institute, Solna, Sweden.

Abstract

Purpose—All uveal melanoma and a fraction of other melanoma subtypes are driven by activation of the $G\alpha_q$ pathway. Targeting these melanomas has proven difficult despite advances in the molecular understanding of key driver signaling pathways in the disease pathogenesis. Inhibitors of $G\alpha_q$ have shown promising preclinical results, but their therapeutic activity in distinct $G\alpha_q$ mutational contexts and *in vivo* have remained elusive.

Experimental Design—We used an isogenic melanocytic cellular system to systematically examine hotspot mutations in *GNAQ* (*e.g.*, G48V, R183Q, Q209L) and *CYSLTR2* (L129Q) found in human uveal melanoma. This cellular system and human uveal melanoma cell lines were used *in vitro* and *in vivo* xenograft studies to assess the efficacy of $G\alpha_q$ inhibition as a single agent and in combination with MEK inhibition.

Results—We demonstrate that the $G\alpha_q$ inhibitor YM-254890 inhibited downstream signaling and *in vitro* growth in all mutants. *In vivo*, YM-254890 slowed tumor growth but did not cause regression in human uveal melanoma xenografts. Through comprehensive transcriptome analysis, we observed that YM-254890 caused inhibition of the MAPK signaling with evidence of rebound by 24 hours and combination treatment of YM-254890 and a MEK inhibitor led to sustained MAPK inhibition. We further demonstrate that the combination caused synergistic growth inhibition *in vitro* and tumor shrinkage *in vivo*.

Conclusions—These data suggest that the combination of $G\alpha_q$ and MEK inhibition provides a promising therapeutic strategy and improved therapeutic window of broadly targeting $G\alpha_q$ in uveal melanoma.

Introduction

Uveal Melanoma (UVM) is the most common intraocular malignancy with approximately 3,000 new cases per year in the U.S. (1,2). Metastatic UVM has a median survival of less than six months and a five-year survival rate of ~15% (3). Unlike cutaneous melanoma, where there has been significant progress in targeted therapy and immunotherapy, there remains no effective systemic therapeutic option for advanced UVM.

UVM is characterized by aberrant activation of the heterotrimeric G-protein alpha-q ($G\alpha_q$) pathway, which canonically activates phospholipase Cβ (PLCB) and downstream effectors,

including inositol 1,4,5-triphosphate (IP_3), diacylglycerol (DAG), and protein kinase C (PKC) (4). Approximately 90% of UVMs harbor activating mutations in two homologous α subunits of $G\alpha_q$ *GNAQ* and *GNA11;* the remaining cases harbor activating mutations in the upstream G protein-coupled receptor (GPCR) cysteinyl leukotriene receptor 2 (*CYSLTR2*) (5–7) and downstream target PLCB4 (8). These mutations are not exclusive to UVM, as they have been identified in a majority of blue nevi, leptomeningeal melanocytic neoplasms (LMNs), hepatic small vessel neoplasms, Sturge-Weber syndrome, and in a small subset of cutaneous and mucosal melanomas (7,9–15). The identification of similar genetic aberrations among these diseases demonstrates the significance of this pathway and the need for effective therapeutic options against it.

The MAPK pathway is an important downstream signaling output of $G\alpha_q$; prior studies highlighted the high levels of MAPK activity in the absence of canonical drivers found in cutaneous melanoma (6,7,16). Despite this, single agent MEK inhibitors (MEKi) have failed to provide clinical benefit (1,17,18). Recent mechanistic studies identified the RAS guanine exchange factor, RasGRP3, as an essential intermediary between $G\alpha_q$ and RAS/MAPK signaling (19,20). Inhibition of RasGRP3 reduced ERK signaling and cell growth further implicating the dependence of MAPK signaling in UVM (19). Promising preclinical studies have pointed to the combination of a pan-PKC inhibitor with MEKi as a potential therapeutic approach. However, clinical applications of these compounds have been hampered by toxicity from pan-PKC inhibition and therefore the lack of therapeutic window (1,17,18,21,22). Direct inhibition of mutant $G\alpha_q$ signaling could potentially circumvent such toxicity and provide an effective therapeutic window and conceivably durable response. The recent development of allele-specific RAS inhibitors revealed mutations in *KRAS*, another small GTPase can continue to cycle between the GTP-GDP states, albeit at reduced rates compared to wild-type (23). In fact, $KRAS^{G12C}$-specific inhibitors, similar to YM, target the GDP-bound state and are efficacious in inhibiting $KRAS^{G12C}$-driven cancers (24–26). These studies have shown that direct targeting of a mutant GTPase is not only possible, but highly efficacious in $KRAS^{G12C}$-driven cancers.

YM-254890 (YM) is a naturally-occurring cyclic depsipeptide that inhibits platelet aggregation by perturbing $G\alpha_q$-mediated Ca^{2+} mobilization (27,28). YM is an allosteric inhibitor that binds to the hydrophobic cleft between two inter-domain linkers of $G\alpha_q$, stabilizing the inactive GDP-bound form by hindering the flexibility of the linkers (29). YM inhibition of $G\alpha_q$ prevents canonical nucleotide exchange; without binding GTP, the protein is unable to activate downstream signaling partners. Studies have shown YM can act as a therapeutic agent for inhibition of platelet aggregation and hypocalcemia (30–32). However, initial studies using overexpression systems indicated YM was unable to inhibit mutant $G\alpha_q^{Q209L}$ (27). The lack of activity was hypothesized to be due to the reduced GTPase activity of the $G\alpha_q^{Q209L}$ mutant and thereby locking the mutant protein in the GTP-bound state similar to the paralogous $G\alpha_s^{Q227L}$ mutant (33). Three recent studies have highlighted the use of FR900359 (FR), an analog of YM, to directly target Q209-mutant $G\alpha_q$. These studies demonstrated FR's ability to inhibit signaling and growth in Q209 mutant UVM cell lines, and efficacy against one human xenograft model (34–36). These reports illustrate direct inhibition of Q209 mutant $G\alpha_q$ as a potential therapeutic avenue for UVM. However, both YM and FR are potent inhibitors of physiologically active wild-type $G\alpha_q$ signaling

(27–29,37), which raises concerns of therapeutic window of YM and FR in targeting mutant $G\alpha_q$ in UVM. Thus, discovery of novel synergistic combinations that can potentiate therapeutic efficacy and broaden the therapeutic window of YM or FR is imperative. Furthermore, there remains a need for a comprehensive understanding of direct $G\alpha_q$ inhibition across the mutational landscape of UVM.

Here, we identified a novel *GNAQ* mutational hotspot, G48, and showed exogenous expression of $GNAQ^{G48V}$, similar to the canonical *GNAQ* mutants, transformed melanocytes. We demonstrated YM effectively inhibited cellular growth and downstream $G\alpha_q$ signaling in four UVM mutants, *GNAQ* (G48V, R183Q, Q209L) and *CYSLTR2* (L129Q). We further confirmed the efficacy of YM in a series of *in vivo* experiments with human UVM cell lines harboring $G\alpha_q^{Q209}$ mutations. Furthermore, transcriptomic and synergistic analysis revealed that together, YM and MEKi led to enhanced and sustained inhibition of MAPK signaling to significantly decrease tumor growth. These results suggest direct $G\alpha_q$ inhibition provides an effective therapeutic strategy in UVM and synergizes with MEKi to further increase therapeutic potential.

Methods

Study approval

MSK-IMPACT testing for UVM patients was ordered by the treating physician who signed informed consent to research protocol (ClinicalTrials.gov, NCT01775072). All animal studies were performed in accordance to MSKCC IACUC 11–12-029.

Drugs and Chemicals

YM-254890 was purchased from Wako Pure Chemical Industries (CAT# 257–00631). MEK162 (binimetinib) was purchased from Array BioPharma Inc. Trametinib was purchased from Selleck Chemicals (Catalog No. S2673).

Mutational Analysis

For the MSKCC uveal melanoma cohort, all patients provided informed consent for tissue procurement and mutational testing, and the study was approved by the institutional review board (ClinicalTrials.gov, NCT01775072). Patients had a confirmed diagnosis of uveal melanoma. A total of 124 specimens from 116 patients were analyzed including 47 specimens from primary UVM and 77 from metastasis (56 liver, 6 lymph node, 5 lung, 10 other). In the 7 patients with multiple samples, the $G\alpha_q$ mutational status were identical. Tumor samples were sequenced using MSK-IMPACTv3, v5, or v6 that captures 341, 410, and 468 genes respectively. The MSK-IMPACT panel includes GNAQ and GNA11 in all versions and CYSLTR2 was added to v6.

For integrative analysis of published cohorts, Level 2 whole-exome mutational data were downloaded from the NIH TCGA server. Processed whole-exome sequencing data from the UNI-UDE (n = 22) and MDACC/MEEI (n = 52) uveal melanoma cohorts and processed whole-genome sequencing data from the CRUK (n = 12) and QIMR (n = 28) cohorts were extracted from the supplementary tables of relevant publications (20–24). For downstream

analysis, we merged the data for 3 duplicate samples present in both the CRUK and TCGA databases and removed 3 samples from the QIMR database that lacked any somatic mutations, leaving 188 samples. The OncoPrint was generated using MSKCC cBioPortal.

Exogenous Gene Expression

For transient transfection experiments in HEK-293T, we used a synthetic gene for codon optimized *CYSLTR2* (5) and WT cDNA for *GNAQ* (cDNA.org). We performed site-directed mutagenesis to generate mutants Q209L, R183Q and G48V using QuickChange (Agilent Technologies) site-directed mutagenesis. HEK-293T cells were transiently transfected with the plasmids encoding for GNAQ WT and mutants subcloned into pcDNA3.1(+) using Lipofectamine according to the manufacturer's instructions. Briefly, 7,000 HEK-293T cells were transfected in low-volume 384-well plates with 11 ng of total DNA/well for 24 hours.

For stable expression in melan-a cells, we employed human cDNAs for *CYSLTR2* and *GNAQ* obtained from Origene, mutagenized using QuickChange and cloned into the retroviral vector MSCV-Puro (Addgene plasmid #68469) (38). $NRAS^{Q61K}$ (Addgene plasmid #49404) and MEKDD (Addgene plasmid #15268) (39) constructs for rescue experiments were purchased from addgene. Retroviral production was performed through transfection of retroviral expression vector with the pCl-Ampho packaging vector with X-tremeGENE 9 (Sigma-Aldrich). QuikChange primers were used to introduce the various mutant constructs. All constructs were confirmed by sequencing. Site directed mutagenesis primers are listed in Supplementary Table S1.

Cell Culture

Mutation dependent melan-a cells were generated by transducing cells with cDNAs in MSCV-PURO (retrovirus) and then selecting cells with puromycin (1μg/ml) for two days. TPA (Sigma-Aldrich) was then withdrawn from cultures. Cells with activating mutations ($CysLT_2R^{L129Q}$, $GNAQ^{G48V/R183Q/Q209L}$, $KRAS^{G12V}$, $BRAF^{V600E}$, and $NRAS^{Q61K}$) continued to proliferate over several passages (>2 weeks). Vector and WT controls were unable to maintain proliferation or pigmentation after a few passages without TPA. All cells were cultured in media containing 10% FBS, L-glutamine (2nM), penicillin (100U/ml), streptomycin (100 μg/ml). Melan-a cells provided by D. Bennett, St. George's Hospital, University of London were cultured in RPMI supplemented with 200nM TPA unless otherwise noted (40). HEK-293T (from ATCC) and A375 cells were cultured in DMEM and UVM cells were cultured in RPMI. All cells tested negative for mycoplasma. Human UVM cell lines Mel202, OMM1.3, and OMM1 were described previously (19) and MP41 was purchased from ATCC (CRL-3297).

Cell Growth Assays and Dose Response Curves

Cell growth and dose response curves for YM were assayed using CellTiter-Glo 2.0 (Promega) and readout on a Glomax Luminometer (Promega). For growth assays, melan-a cells were seeded in the absence of TPA, 1,000 cells/well in a 96-well plate and then counted on days 1, 3, and 6. Growth assays were baselined to day 1 readings. For dose response curves melan-a and human UVM cells were seeded 1,000–3,500 cells/well in a 96-well plate and treated 24 hours later with YM for 5 days. Data was baselined to vehicle. Growth assays

and dose response curves were analyzed and IC_{50} values calculated using GraphPad Prism 7.0 software. Data shown is representative of at least three independent experiments with at least three technical replicates.

Crystal Violet Growth Assay

Cells were seeded in 12- or 6-well plates, media and drug were replenished every two days. Cells were washed twice with ice cold 1X PBS, fixed with ice cold 100% methanol, and stained with 0.5% crystal violet (sigma) solution in 25% ethanol. Plates were imaged with a GELCOUNT (Oxford Optronix).

Drug Synergy Analysis

Synergy assays were performed in 96 well plates (1,000–3,000 cells/well) for 5 days with Trametinib and YM, readout by CellTiter-Glo 2.0. Viability was baselined to vehicle (100%), input into Combenefit software to obtain HSA synergy and viability plots (41). Data shown is representative of at least three independent experiments with three technical replicates.

Mouse experiments

For melan-a allograft studies, 2.0×10^6 cells were resuspended in 100μL of 1:1 mix of RPMI media and Matrigel (BD Biosciences) and subcutaneously injected into 6–8-week-old C57BL/6J mice (Jackson Laboratory). For Mel202 xenograft studies, 3.0×10^6 cells were injected into 6–8-week-old CB17-SCID mice (Taconic). Tumor sizes were measured twice a week with calipers starting from three weeks post graft and were calculated using the following formula: tumor volume = (D2 × d2× h2)/6, whereby D, d and h refers to long diameter, short diameter and height of the tumor, respectively. Treatment began at a tumor size of ~100mm^3. Mice were treated with YM-254890 (daily intraperitoneal injection), binimetinib (twice daily oral gavage), a combination of both drugs, or a matched vehicle (0.5% DMSO in 1X PBS and 1% Carboxymethyl cellulose + 0.5% Tween 80 in ddH_2O, or both, respectively). Mice were treated for five days and then given two days for recovery for the length of the experiment. Mice were euthanized in response but not limited to the following: tumor ulceration, tumors located too close to the trunk of the mice to impede movement and blood flow, and tumor burden. For all experiments, mice were grafted double flank, except Fig. 6A (single flank).

Luciferase Imaging

OMM1.3 cells were transduced with pBMN (CMV-copGFP-Luc2-Puro) for luciferase expression (Addgene plasmid # 80389) (42). OMM1.3 xenografts were setup the same as Mel202 grafts described above. Treatment was started 3 days after grafting, following the methods described above. Mice were injected with 15mg/ml D-luciferin potassium salt (GoldBio) in 1X PBS and imaged 15 minutes later using Xenogen IVIS Spectrum. The raw photon flux was calculated using Living Image 4.4 Software and baselined to day 1 readings.

Western Blotting Analysis

Cell lysates were harvested after indicated treatments as previously described (5,19). For western blots of OMM1.3 tumors, mice were treated once (q.d.) with vehicle, YM, binimetinib, or combo and then scarified four hours later. For western blots of Mel202 tumors, mice were treated with vehicle, YM (q.d.), binimetinib (b.i.d), or combo for a week and then scarified four hours after the last treatment. Tumor lysates were generated as previously described (19). Primary antibodies were incubated at a 1:1,000 dilution, unless noted otherwise. Western blot antibodies are listed in Supplementary Table S2 and raw blots are shown in Supplementary Fig. S7.

Immunohistochemistry

All tissues were fixed at 4°C overnight in 4% paraformaldehyde. Tissue processing, embedding, sectioning, and H&E staining were performed by Histoserv. Staining was done as previously described (19). IHC antibodies and dilutions are listed in Supplementary Table S3.

RNA Isolation and qRT-PCR

RNA was extracted from cells using Trizol (Invitrogen) following the manufacturers standard Trizol extraction protocol. 2 μg of RNA from each sample was reverse transcribed to cDNA using the High Capacity cDNA Reverse Transcription Kit (Applied Biosystems). Power SYBR Green PCR Master Mix (Applied Biosystems) was then used for PCR on a QuantStudio 6 Flex System (Applied Biosystems). Expression was normalized to ribosomal protein RPL27. Relative expression of mRNA was plotted as $2^{-\Delta\Delta Ct}$ and each experiment was performed in triplicate and repeated in at least three independent experiments. qRT-PCR primers are listed in Supplementary Table S4.

Bioinformatics Analysis

TCGA uveal melanoma (UVM) and skin cutaneous melanoma (SKCM) mutational and RNA-seq data were download from cBioPortal (www.cbioportal.org) using the PanCancer Atlas Version. The six SKCM samples with GNAQ or GNA11 Q209L mutations are TCGA-RP-A6K9–06, TCGA-RP-A690–06, TCGA-ER-A3ET-06, TCGA-ER-A3ES-06, TCGA-ER-A2NF-06, TCGA-ER-A2NF-01. All RNA-seq was performed by MSKCC genomics core facility using poly-A capture. The libraries were sequenced on an Illumina HiSeq-2500 platform with 50 bp paired-end to obtain a minimum yield of 40 million reads per sample. The sequence data for all melan-a cells were mapped to the mouse reference genome (GRCm38), whereas, Mel202 and OMM1.3 were mapped to the human reference genome (GRCh38) using STAR v2.330 (43). Gene counts were quantified using STAR to Ensembl gene annotations GRCm38.91 and GRCh38.90 for mouse and human samples, respectively. Counts were r-log transformed using DESeq2 (44). Hierarchical clustering and heatmaps of wild-type melan-a cells grown in TPA and $GNAQ^{Q209L}$ and $KRAS^{G12V}$ transduced melan-a cells grown without TPA was performed on r-log transformed genes with STDEV>1.5 using Partek Genomics Suite. K-means clustering and heatmaps of drug treated melan-a and human uveal melanoma cells were performed on r-log transformed, Z-scored (mean = 0, stdev = 1), and then partition clustered (k-means) were performed using Partek Genomics

Suite. Sum Z-scores were calculated by adding transformed gene expression data from the specified gene signatures. Gene sets are listed in Supplementary Table S5. Cluster and gene set (Hallmark) enrichment analysis were obtained from https://www.gsea-msigdb.org/gsea/index.jsp and are shown in Supplementary Table S6–S11. Raw and processed data are deposited in Gene Expression Omnibus (GEO) Accession #: GSE152705 and GSE160112.

IP_1 Accumulation Assay

IP_1 concentrations in transfected HEK-293T cells, stably transduced melan-a cells, and uveal melanoma cells were measured using a competitive homogenous time resolved fluorescence (HTRF) assay (CisBio). Briefly, 7,000 transiently transfected HEK-293T cells, 5,000 melan-a cells and 5,000 uveal melanoma cells were seeded in low-volume 384-well plates in 7 μL media for 24 hours prior to YM treatment. Cells were then treated with various concentrations of YM at 37°C for 3 or 24 hours. 1 hour and 45 minutes prior lysis, cells were supplemented with 1X Stimulation Buffer provided by the manufacturer (HEPES 10 mM, CaCl2 1 mM, MgCl2 0.5 mM, KCl 4.2 mM, NaCl 146 mM, glucose 5.5 mM, LiCl 50 mM, pH 7.4) with 0.2% BSA and 50 mM of LiCl (to prevent IP_1 degradation). Following incubation, cells were lysed by addition of 3 μL/well of d2-labeled IP_1 analogue as the fluorescence acceptor and the Terbium cryptate-labeled anti-IP1 mAb as the fluorescence donor, diluted in the kit-supplied lysis buffer. The plates were incubated overnight at RT and time-resolved fluorescence signals were read using the BioTek Synergy NEO plate reader (BioTek Instruments, Winooski, VT) at 620 nm and 665 nm. Results were calculated as a 665nm/620nm signal ratio, and IP_1 concentrations were interpolated from a standard curve prepared using the supplied IP_1 calibrator. Results are shown as IP_1 (nM). Dose response curves and bar graphs were analyzed using GraphPad Prism 7.0 software.

Statistical analysis

All statistical comparisons were done with Graphpad Prism 7.0 software and used a two-tailed Student's t-test for comparison between groups. Data is shown as the mean ± SEM (unless otherwise noted) from triplicate samples from at least three independent experiments. P less than 0.05 was used to designate significance. Significant differences between groups are indicated by $P > .05$; ns, $P < 0.05$; *, $P < 0.005$; **, $P < 0.0005$; ***, $P < 0.0001$, ****.

Results

$G\alpha_q$ mutations occur at three hotspot residues that are known to perturb GTP hydrolysis

We examined the $G\alpha_q$ pathway mutations from a series of 116 consecutive patients with UVM seen at Memorial Sloan Kettering Cancer Center (MSKCC) and who had undergone clinical sequencing on the MSK-IMPACT platform (45). Similar to previously reported cohorts, 107 of 116 patients harbored mutually exclusive activating mutations in either *GNAQ* or *GNA11* and two patients had a $CYSLTR2^{L129Q}$ mutation (Fig. 1A) (5). For *GNAQ*, in addition to previously known recurrent mutations at amino acids Q209 and R183, one sample harbored a novel G48L mutation. To further evaluate the $GNAQ^{G48}$ mutation, we next integrated 188 uveal melanoma patients from 5 published whole-exome or whole-genome uveal melanoma cohorts (8,46–49). We identified two patients with $GNAQ^{G48L}$ and

one patient with a *GNAQ*^{G48V} mutation, indicating G48 as a third mutational hotspot in *GNAQ* (Fig. 1B). The codon G48 resides in the phosphate binding loop (P-loop) of $G\alpha_q$ and is paralogous to codon G12 in RAS GTPases, which is frequently mutated in various cancers (23). Furthermore, the paralogous G47V mutation in *GNAS* exhibits constitutive activity (33). Structural studies of active $G\alpha_q$ illustrate G48 of the P-loop, R183 of switch I, and Q209 of switch II are in spatial proximity adjacent to the nucleotide-binding pocket (Fig. 1C) (50), indicating mutations in G48, like Q209 and R183 would hinder GTPase activity.

Generation of isogenic melanocytes dependent on mutations found in UVM

To determine the role of distinct UVM driver mutations in a genetically defined context, we stably expressed human cDNAs encoding *CYSLTR2*^{L129Q}, *GNAQ*^{G48V}, *GNAQ*^{R183Q}, *GNAQ*^{Q209L}, WT controls, as well as *BRAF*^{V600E}, *KRAS*^{G12V}, and *NRAS*^{Q61K} in melan-a cells (Supplementary Fig. S1A and S1B) (40). BRAF^{V600E}, KRAS^{G12V}, and NRAS^{Q61K} hyperactivate the RAS-RAF-MEK-ERK kinase (MAPK) signaling pathway, distinct from the GPCR-$G\alpha_q$-PLCβ signaling axis. Melan-a cells are immortalized mouse melanocytes that require media supplemented with 12-O-tetradecanoyl-phorbol-13-acetate (TPA), a DAG analog, for continued proliferation and are characterized by pigmentation and melanocytic morphology (5,40). After TPA withdrawal, melan-a cells expressing empty vector, *CYSLTR2*^{WT} or *GNAQ*^{WT} lost pigmentation and eventually growth arrested (Fig. 1D and 1E; Supplementary Fig. S1C). However, cells expressing activating mutations of *GNAQ* and *CYSLTR2* exhibited TPA-independent growth and enhanced melanocytic features (e.g. dark pigmentation, enlarged melanosomes). Interestingly, expression of *BRAF*^{V600E}, *KRAS*^{G12V}, and *NRAS*^{Q61K} that hyperactivate MAPK signaling also conveyed TPA-independence but failed to maintain pigmentation (Fig. 1D and 1E; Supplementary Fig. S1C and S1D).

We next examined the ability of $G\alpha_q$ to stimulate PLCβ and generate IP_3, by measuring accumulation of the IP_3 degradation product IP_1. Melan-a cells expressing *CYSLTR2*^{L129Q} and all three *GNAQ* mutations exhibited enhanced IP_1 accumulation, whereas the *CYSLTR2*^{WT}-, *GNAQ*^{WT}-, *BRAF*^{V600E}-, *KRAS*^{G12V}-, and *NRAS*^{Q61K}-expressing cells did not, indicating that this cellular system faithfully recapitulates the distinct signaling pathways driven by $CysLT_2R$ and $G\alpha_q$ oncoproteins (Fig. 1F; Supplementary Fig. S1E). Western blot analysis of melan-a cells following TPA-withdrawal showed that UVM associated $CysLT_2R$ and $G\alpha_q$ oncoproteins maintained expression of melanocyte markers MITF, c-KIT, TRP2/DCT, and RASGRP3 (UVM specific), whereas wild-type CYSLTR2^{WT}, GNAQ^{WT}, KRAS^{G12V}, and NRAS^{Q61K} did not (Fig. 1G; Supplementary Fig. S1F). In TCGA datasets, we found these genes (MITF, KIT, DCT, and RASGRP3) were expressed higher in uveal melanoma (UVM) and $G\alpha_q$ -mutated skin cutaneous melanoma (SKCM) compared to RAS/RAF mutated SKCM (Supplementary Fig. S1G), suggesting that the engineered melan-a cells capture important oncogene-specific biology of human melanomas (5,19).

To determine the transcriptome response to expression of activated $G\alpha_q$ and RAS/RAF pathway in melan-a cells, we performed RNA-seq in wild-type melan-a cells grown in TPA, melan-a expressing *GNAQ*^{Q209L} and melan-a expressing *KRAS*^{G12V} cells after TPA-withdrawal. Unsupervised hierarchical clustering showed wild-type cells in TPA were more

similar with *GNAQ*^{Q209L} cells than *KRAS*^{G12V} cells, consistent with direct $G\alpha_q$ signaling to phospholipase C-beta to generate DAG and IP3 (Supplementary Fig. S1H). To determine pathways activated in these melan-a lines, we performed enrichment analysis of gene ontology (GO), Hallmark, and KEGG gene sets as well as custom gene sets defined by genes differentially expressed between human $G\alpha_q$ vs BRAF/NRAS/KRAS mutated melanoma from TCGA uveal and cutaneous melanoma datasets (46,51) and by genes differentially expressed in genetically engineered mouse melanoma in Bap1^{KO};Gna11^{Q209L} vs Bap1^{KO};BRAF^{V600E} mice (19). We found that *GNAQ*^{Q209L} melan-a cells had increased expression of genes in human $G\alpha_q$ mutated melanomas and mouse Bap1^{KO};Gna11^{Q209L} tumors while *KRAS*^{G12V} melan-a cells had increased expression of genes in human RAS/RAF mutated tumors and mouse Bap1^{KO};Braf^{V600E} tumors (Supplementary Fig. S1I). In addition gene sets including calcium mediated signaling and melanogenesis were strongly enriched in GNAQ^{Q209L} cells, whereas MAPK signaling was enriched in KRAS^{G12V} cells (Supplementary Fig. S1I). (19). These data indicate $G\alpha_q$ activation generates a distinct oncogenic phenotype that maintains melanocyte lineage specification, and is consistent with previous observations in genetically engineered murine models of UVM (19,52). This system of engineered mutant oncoprotein-transformed melanocytes allows for context-relevant systematic evaluation of $G\alpha_q$-pathway activating mutations that are not available in human cancer cell lines or patient-derived xenograft (PDX) UVM models.

YM-254890 inhibits mutation dependent melan-a cells *in vitro* and *in vivo*

We next determined the ability of YM to inhibit the activity of distinct UVM mutations. Since YM is thought to stabilize the GDP-bound state of $G\alpha_q^{WT}$, we hypothesized $CysLT_2R^{L129Q}$ would be particularly sensitive to YM. First, we tested the ability of YM to inhibit $G\alpha_q$ signaling in a panel of HEK-293T cells transfected with oncoprotein cDNA constructs and assayed the dose response of IP_1 accumulation 24-hours following treatment of YM. In this system, $CysLT_2R^{L129Q}$ and $G\alpha_q^{G48V}$ appeared to be most sensitive to YM with subnanomolar potency (Supplementary Fig. S2A). $G\alpha_q^{R183Q}$ was ~20-fold less sensitive to YM compared to $CysLT_2R^{L129Q}$ and $G\alpha_q^{G48V}$, whereas $G\alpha_q^{Q209L}$ was the least sensitive to YM and its signaling was incompletely inhibited within 24-hour YM treatment, consistent with previous reports (Supplementary Fig. S2A) (27).

Transient transfection experiments in HEK-293T cells result in non-physiologic overexpression of oncoproteins and can lead to misleading observations. In the more physiologic context of $G\alpha_q$ pathway mutant-transformed melan-a cells, when we assayed IP_1 after 3 hours of treatment, rapid reduction of IP_1 was observed with UVM oncoproteins except $G\alpha_q^{Q209L}$, which achieved only half-maximal inhibition (Fig. 2A). Interestingly, 24-hour treatment with YM completely inhibited IP_1 accumulation across all UVM activating mutants, including $G\alpha_q^{Q209L}$. $CysLT_2R^{L129Q}$ and $G\alpha_q^{G48V}$ were most sensitive to YM, whereas $G\alpha_q^{R183Q}$ and $G\alpha_q^{Q209L}$ mutants were approximately 10-fold less sensitive (Fig. 2A). These data suggest activating $G\alpha_q$ mutants, while prominently GTP-bound, undergo GTP hydrolysis, albeit presumably at decreased levels compared to wild-type, allowing for YM to bind in the $G\alpha_q$ GDP-state, reminiscent of covalent KRAS^{G12C} inhibitors (24–26,29).

We next assayed the effect of YM on downstream $G\alpha_q$ signaling, including RASGRP3 phosphorylation by PKC, MAPK signaling by CRAF, MEK, and ERK phosphorylation and cyclin D1 expression that integrates signaling to promote cell cycle progression. YM inhibited these downstream signaling targets, with slower kinetics in $G\alpha_q^{R183Q}$ and $G\alpha_q^{Q209L}$ expressing cells compared to $CysLT_2R^{L129Q}$ and $G\alpha_q^{G48V}$ expressing cells (Fig. 2B), consistent with the IP_1 biochemical assay. Since TPA is a DAG analog and acts downstream of $G\alpha_q$, supplementing it in the media restored downstream signaling targets 24 hours after YM treatment (Fig. 2B). YM was ineffective in inhibiting MAPK signaling in $BRAF^{V600E}$, $KRAS^{G12V}$, and $NRAS^{Q61K}$-expressing cells (Supplementary Fig. S2B), confirming the specificity of YM to $G\alpha_q$ inhibition. Expressing $KRAS^{G12V}$ in $CysLT_2R^{L129Q}$ and $G\alpha_q^{Q209L}$ melan-a cells rescued YM-mediated MAPK inhibition (Supplementary Fig. S2E). We next examined if YM could effectively inhibit TPA-independent cell growth in the engineered melan-a cells. Consistent with IP_1 accumulation, all UVM activating mutants were highly sensitive to YM. $CysLT_2R^{L129Q}$ and $G\alpha_q^{G48V}$ cells exhibited low-nanomolar sensitivity to YM, and the $G\alpha_q^{R183Q}$- and $G\alpha_q^{Q209L}$-expressing cells were modestly less sensitive, whereas the $BRAF^{V600E}$, $KRAS^{G12V}$, and $NRAS^{Q61K}$ -expressing cells were insensitive (Fig. 2C; Supplementary Fig. S2C). TPA supplementation or $KRAS^{G12V}$ expression rescued YM-mediated growth inhibition in $CysLT_2R^{L129Q}$-expressing cells (Supplementary Fig. S2D).

We performed pilot pharmacokinetic studies suggesting YM has a short serum half-life in mice (data not shown). However, given its potency, YM may engage and inhibit $G\alpha_q$ more durably. We thus performed a pharmacodynamic study examining downstream signaling in $CysLT_2R^{L129Q}$ cells allografted into C57BL/6J mice. After a single dose of YM given at 7.5 mg kg^{-1} intraperitoneally, we observed inhibition of downstream signaling in $CysLT_2R^{L129Q}$ tumors as early as 30 minutes (Fig. 2D). By 24 hours, a sustained decreased in ERK phosphorylation and cyclin D was observed despite rebound of CRAF phosphorylation. We observed a paradoxical increase in RASGRP3 phosphorylation levels which may indicate feedback activation in this model.

Given these data, we proceeded to dose YM daily and assessed efficacy. We observed YM significantly inhibited tumor growth of $CysLT_2R^{L129Q}$ or $G\alpha_q^{Q209L}$ allografts (Fig. 2E and 2F). Importantly, YM treatment did not cause adverse effects such as weight loss (Supplementary Fig. S2F and S2G). These data suggest YM is a highly selective inhibitor against $G\alpha_q$ signaling and can effectively inhibit proliferation both *in vitro* and *in vivo*.

YM-254890 inhibits growth of human UVM cells and xenograft models

Given the sensitivity of all three activating hotspot mutations to YM, including the most common $GNAQ^{Q209L}$ mutation, in the melan-a system, we proceeded to study the effect of YM on a panel of human UVM cell lines that harbor $GNAQ^{Q209L/P}$ or $GNA11^{Q209L}$ mutations and A375 ($BRAF^{V600E}$) cutaneous melanoma cell line as control. UVM cells exhibited high basal activity of IP_1 accumulation, which was inhibited upon YM treatment at 24 hours (Fig. 3A; Supplementary Fig. S3A). Analysis of downstream signaling showed RASGRP3, MAPK output, and cyclin D1 proteins were inhibited in UVM cells, but not in A375 cells, upon treatment with YM (Fig. 3B; Supplementary Fig. S3B). Expressing

$NRAS^{Q61K}$ or MEK^{DD} in UVM cells completely rescued YM-mediated MAPK inhibition (Supplementary Fig. S3G). In OMM1.3 and Mel270 cells, treatment with YM rapidly inhibited the MAPK pathway while suppression of the intermediary target, p-RASGRP3, required prolonged drug exposure. In contrast, YM treatment in Mel202 cells showed potent inhibition of p-RASGRP3 at early time points, but the MAPK pathway was only mildly inhibited; p-ERK1/2 rebounded by 24 hours. These results indicate UVM cells may have different wiring downstream of $G\alpha_q$. Regardless, YM potently and effectively inhibited cell viability in $G\alpha_q$ mutant UVM cell lines but not A375 cells (Fig. 3C; Supplementary Fig. S3C and S3D). TPA supplementation, $NRAS^{Q61K}$, or MEK^{DD} expression rescued YM-mediated growth inhibition in UVM cells (Supplementary Fig. S3C, S3E, and S3F).

We next used a UVM xenograft model to test the efficacy of YM *in vivo*. In mice with xenografts of OMM1.3 cells, YM inhibited tumor formation compared to vehicle and no adverse weight loss was observed (Fig. 3D; Supplementary Fig. S3H). Taken together, these data indicate that $G\alpha_q$ inhibition is effective against human UVM xenografts *in vivo*, in agreement with previously reported data using FR (53).

$G\alpha_q$ inhibition and MEKi synergistically sustain MAPK inhibition and suppress growth in UVM models

To gain further mechanistic insight, we compared the transcriptional response to YM with that of trametinib treatment for 4- or 24-hours in the $CysLT_2R^{L129Q}$ melan-a cells. Perturbed genes were partitioned into six clusters by *k*-means clustering algorithm (Fig. 4A). Genes downregulated by either YM or trametinib behaved similarly to one another (Clusters 1, 2, 3), whereas upregulated genes were distinct (Clusters 4, 5, 6). We then computed the top five GSEA HALLMARK gene set overlaps with each cluster to better understand the impact of treatment on these clusters (Supplementary Fig. S4A). YM, similar to trametinib, effectively inhibited the cell cycle progression (E2F targets) of $CysLT_2R^{L129Q}$ cells at 24-hours (cluster 1; Fig. 4B). However, trametinib more potently suppressed KRAS and inflammatory signaling than YM (cluster 2; Fig. 4B; Supplementary Fig. S4A). To further understand the suppression of KRAS genes, we used a 52-gene set comprised of genes rapidly downregulated by MEK inhibition in melanoma cells (54), PRATILAS_MAPK signature. This gene signature was downregulated by both YM and trametinib at 4 hours, but by 24 hours, genes rebounded with YM treatment while trametinib further suppressed this gene signature (Fig. 4C). Specifically, this rebound pattern was seen in MAPK signaling output genes *DUSP6* and *SPRY2/4* (Fig. 4D). This suggests that YM does not durably suppress MAPK signaling at 24 hours, potentially limiting therapeutic effect.

This prompted us to ask whether YM could be used in combination with MEKi to prevent potential MAPK rebound and induction. In our melan-a cellular system, we found significant synergy in an HSA assay between YM and trametinib in cells dependent on *CYSLTR2* or *GNAQ* mutants but not in melan-a cells still dependent on TPA (Fig. 4E; Supplementary Fig. S4B). Long term treatment of YM plus trametinib greatly reduced proliferation of $CysLT_2R^{L129Q}$ cells at 26 days compared to single agent treatments (Fig. 4F). In melan-a cells with TPA, only trametinib showed long term effects on proliferation. Combination treatment in $CysLT_2R^{L129Q}$ melan-a cells led to rapid MAPK signaling

inhibition that was sustained for 72 hours, whereas p-ERK had returned to basal levels in single treatment groups (Fig. 4G). To further investigate these findings, we used UVM cell lines to assess the effect of YM and MEKi on viability, transcriptomics, and signaling. We performed HSA synergy assays on four UVM cell lines and found significant synergy between YM and trametinib (Fig. 5A; Supplementary Fig. S5A). Growth assays in these UVM cell lines showed variable sensitivity to either YM or MEKi, but combination of the two drugs lead to fewer colonies than single agents in all UVM cells (Fig. 5B). However, $BRAF^{V600E}$ mutant A375 cells did not show synergy and only showed sensitivity to MEKi and combination with YM did not lead to a decrease in colonies (Supplementary Fig. S5B and S5C).

To better understand the synergistic effect of the combination, we performed RNA-seq in two human UVM cell lines treated with vehicle, single agent YM or trametinib, or a combination of both for 24 hours (Supplementary Fig. S5D and S5E). Similar to the melan-a cells, we observed trametinib suppressed the PRATALIS_MAPK gene signature with a greater effect than YM (Fig. 5C). Combination resulted in more dramatic gene expression changes when compared to single agent or vehicle and also led to greater inhibition of MAPK, cell cycle, and MYC gene sets, with the exception of cell cycle in Mel202 cells (Fig. 5C; Supplementary Fig. S5D and S5E). Specifically, combination led to greater suppression of MAPK signaling output genes *DUSP6* and *SPRY2/4* (Fig. 5D). This transcriptomic data indicates that YM and trametinib have very similar effects on gene expression, however combination of the drugs further enhances the effects on gene expression.

We next determined the effects of YM, trametinib and combination treatment on signaling. In Mel202 cells, YM treatment alone inhibited RASGRP3, CRAF, and MEK phosphorylation at all time points but downstream ERK and cyclin D inhibition was modest (Fig. 5E). Trametinib treatment alone inhibited ERK phosphorylation at 24 hours with rebound by 48 hours, and combination treatment sustained robust inhibition at all timepoints. Similarly, in OMM1.3 and MP41 cells, YM single agent was very effective at inhibiting RASGRP3, CRAF, and MEK phosphorylation but ERK phosphorylation rebounded by 72 hours (Fig. 5F and 5G). Combination treatment led to sustained inhibition of ERK phosphorylation and cyclin D. Expression of $KRAS^{G12V}$ in OMM1.3 cells was sufficient to rescue YM-mediated p-ERK inhibition, but not trametinib- or combination-mediated p-ERK inhibition (Supplementary Fig. S5F). These data suggest that $G\alpha_q$ and MEK inhibition are more effective against UVM cell growth and signaling than single agents, indicating that combination therapy may have an increased clinical benefit.

In vivo combination of YM-254890 and binimetinib inhibits tumor growth and potently suppresses the MAPK pathway

We tested the combination of YM with an FDA-approved MEK inhibitor binimetinib *in vivo*. Using the $G\alpha_q^{Q209L}$ melan-a allograft model, we tested the combination on immunocompetent C57BL/6J mice treated over the course of 20 days. Mice treated with YM or binimetinib alone had a significant inhibition in tumor growth, with about a two-fold increase compared to day one size (Fig. 6A). However, combination treatment led to significant tumor reduction compared to vehicle or single agents (Fig. 6A). Similarly, we

found that the combination greatly reduced tumor growth in the $CysLT_2R^{L129}$ allograft model. (Fig. 6B). No treatment group resulted in weight loss (Supplementary Fig. S6A and S6B). These experiments show that together, YM and MEKi further reduced tumor burden in allograft models driven by two different activating mutations found in patients.

In the OMM1.3 luciferase xenograft model, single agent treatments did inhibit growth, but combination treatment decreased tumor luminescence by 1000-fold, and we were unable to identify the grafts at the end of treatment (Fig. 6C; Supplementary Fig. S6C). OMM1.3 tumors from mice treated for 4 hours showed that combination potently inhibited both PKC and MAPK signaling (Fig. 6D). Single agent binimetinib inhibited p-ERK but increased p-MEK, typical of MAPK feedback (55), whereas YM treatment potently inhibited RASGRP3 and MAPK signaling despite minimal changes in ERK phosphorylation (Fig. 6D). Immunohistochemistry of these OMM1.3 tumors showed no change in Ki67 staining, most likely due to the short treatment time, but did show a dramatic decrease in p-S6R staining (Supplementary Fig. S6E). We also tested this combination in Mel202 xenografts, which exhibit much slower *in vivo* growth. YM and binimetinib both showed a tumor reduction of about 30% whereas combination led to a greater than 75% average tumor reduction (Fig. 6E; Supplementary Fig. S6D). Tumors from Mel202 xenografted mice, treated for one-week, displayed low basal levels of activated RASGRP3, CRAF, and MEK but did have measurable p-ERK levels (Fig. 6F). YM treatment decreased p-RASGRP3 and downstream ERK signaling, while p-ERK remained unchanged, whereas binimetinib potently inhibited p-ERK and downstream targets but caused rebound in p-RASGRP3, p-CRAF, and p-MEK. Combination treatment suppressed the reactivation of p-MEK and p-CRAF compared to single agent binimetinib and lead to more potent inhibition of p-ERK and p-P90RSK. Immunohistochemistry of these Mel202 tumors show residual Ki67 and p-S6R staining and no significant p-ERK staining in combination treated mice (Fig. 6G), which corroborates the western blot analysis. These *in vivo* data indicate that combination treatment in mice is feasible, highly active, and more efficacious than single agent YM or MEKi.

Discussion

Advances in targeted therapy have shown that direct inhibition of mutated oncoproteins, such as EGFR, KIT, KRAS and BRAF can be highly efficacious, due to the high selectivity against the oncoprotein over wild-type. Inhibition of downstream signaling is more challenging and often limited by on-target toxicity and narrow therapeutic window. UVM is molecularly defined by mutational activation of the $G\alpha_q$ pathway and harbor low mutational burden suggesting effective direct $G\alpha_q$ inhibition could have high efficacy. Compared to kinases, rational design of drugs against mutant GTPases, such as $G\alpha_q$ and RAS, have been challenging for a number of reasons: activating mutations in GTPases are enzymatically impaired whereas those in kinases are enzymatically hyperactive; GTPases activate downstream effectors through protein-protein interactions whereas kinases activate effectors through enzymatic modification; the abundance of intracellular GTP also makes it difficult to design high-affinity inhibitors that can directly access and bind to the GTP-binding pocket (56). Therefore, GTPases cannot be targeted through inhibition of enzymatic activity but require allosteric drugs that affect conformation or effector binding. Nature has evolved strategies that target human GTPases, including brefeldin A that inhibits ARF, pertussis

toxin inhibits $G\alpha_i$, YM from bacteria and FR from the plant *Ardisia crenata* inhibit $G\alpha_q$. In each case, the inhibitor functions through stabilization of the GDP-bound inactive or transitional states, suggesting that active cycling is critical for inhibitor function.

The varying susceptibility to YM across our panel of $G\alpha_q$ mutants underscores the biochemical differences of these mutants. These novel findings have strong parallels to mutant RAS proteins. Structurally, RAS and $G\alpha_q$ share homologous mutational “hotspots”, Q61/Q209 and G12/G48, respectively. Interestingly, codon Q61 mutations in *KRAS* are thought to be more active than those at codon G12, with higher rates of intrinsic nucleotide exchange and a greater reduction of intrinsic hydrolysis (23). This is consistent with our observations of increased IP_1 output for $G\alpha_q^{Q209L}$ and could also explain the differences in YM sensitivity we see between $G\alpha_q$ mutants. The GDP-bound state of $G\alpha_q^{Q209L}$ may be short-lived compared to $G\alpha_q^{G48V}$ or wild-type $G\alpha_q$ in $CysLT_2R^{L129Q}$ cells, making it less susceptible to inhibition by YM. While YM effectively inhibits the panel of mutants both *in vitro* and *in vivo*, these biochemical differences require foresight clinically.

As observed in *RAS*-mutant tumors, allele-specific inhibitors show limited efficacy as monotherapies and will require combinations with other inhibitors (23). As oncogenic mutations in UVM activate RAS proteins through RasGRP3, we hypothesize resistance mechanisms to direct inhibitors of $G\alpha_q$ could occur through reactivation of the MAPK pathway. In fact, compared to trametinib, we observed YM fail to fully suppress the MAPK gene signature. Therefore, the combination strategy of YM plus MEKi could prevent reactivation and durably suppress MAPK signaling. This strategy may also circumvent some of the disadvantages of targeting wild-type $G\alpha_q$, which allows for lower doses of YM and MEKi and broadens the therapeutic window for maximal clinical benefit.

Our work and recent studies highlight the possibility of directly targeting oncogenic $G\alpha_q$ signaling characteristic of UVM and the importance of pursuing this strategy further (34–36). One important limitation of this study and others is the lack of testing $G\alpha_q$ inhibition in liver metastasis models of UVM. Although these models are technically difficult and typically require intrasplenic injection of cells it is important to understand $G\alpha_q$ inhibition efficacy in the liver tumor microenvironment. Recently, complete synthesis of YM as well as FR, and novel analogs of each have been reported (37,57–60) and a large toolbox of $G\alpha_q$ inhibitors will likely soon be available.

In summary, we showed cells harboring activating mutations at one of three residues in *GNAQ,* as well as wild-type $G\alpha_q$ driven by $CYSLTR2^{L129Q}$ were exquisitely sensitive to YM treatment. Transcriptomic and synergy analysis revealed combination of YM with MEKi provides an efficacious and durable response. Our work demonstrates that combination of YM and MEKi leads to enhanced reduction in tumor growth and signaling in UVM, making it an ideal treatment strategy to pursue clinically.

Supplementary Material

Refer to Web version on PubMed Central for supplementary material.

Acknowledgements

This work was supported by the Ruth L. Kirschstein National Research Service Award (NRSA) Individual Predoctoral Fellowship from the NCI (1F31CA236030–01A1, TDH), MSKCC Support Grant/Core Grant (P30 CA008748) and grants from the NCI (K08CA140946 YC; R01CA193837, YC; P50CA092629, YC; P50CA140146, PC; K08CA151660, PC; DP2 CA174499, PC), US DOD (W81XWH-10–1-0197, PC), Prostate Cancer Foundation (YC), Starr Cancer Consortium (YC, PC), Geoffrey Beene Cancer Research Center (YC, PC), Gerstner Family Foundation (YC), Bressler Scholars Fund (YC), and Cycle for Survival (YC). B.S.T. is supported by R01 CA204749 and R01 CA245069. EC was supported by the Francois Wallace Monahan Fellowship and the Thomas Haines Fellowship. We thank the Robertson Therapeutic Development Fund for partial support.

References

1. Chattopadhyay C, Kim DW, Gombos DS, Oba J, Qin Y, Williams MD, et al. Uveal melanoma: From diagnosis to treatment and the science in between. Cancer. 2016;2299–312. [PubMed: 26991400]
2. Chua V, Lapadula D, Randolph C, Benovic JL, Wedegaertner PB, Aplin AE. Dysregulated GPCR Signaling and Therapeutic Options in Uveal Melanoma. Mol Cancer Res. 2017;
3. Jovanovic P, Mihajlovic M, Djordjevic-Jocic J, Vlajkovic S, Cekic S, Stefanovic V. Ocular melanoma: An overview of the current status. Int J Clin Exp Pathol. 2013;6:1230–44. [PubMed: 23826405]
4. Goldsmith ZG, Dhanasekaran DN. G Protein regulation of MAPK networks. Oncogene. 2007.
5. Moore AR, Ceraudo E, Sher JJ, Guan Y, Shoushtari AN, Chang MT, et al. Recurrent activating mutations of G-protein-coupled receptor CYSLTR2 in uveal melanoma. Nat Genet. 2016;
6. Van Raamsdonk CD, Griewank KG, Crosby MB, Garrido MC, Vemula S, Wiesner T, et al. Mutations in GNA11 in Uveal Melanoma. N Engl J Med. 2010;
7. Van Raamsdonk CD, Bezrookove V, Green G, Bauer J, Gaugler L, O'Brien JM, et al. Frequent somatic mutations of GNAQ in uveal melanoma and blue naevi. Nature. 2009;
8. Johansson P, Aoude LG, Wadt K, Glasson WJ, Warrier SK, Hewitt AW, et al. Deep sequencing of uveal melanoma identifies a recurrent mutation in PLCB4. Oncotarget [Internet]. 2016;7:4624–31. Available from: http://www.ncbi.nlm.nih.gov/pubmed/26683228
9. Möller I, Murali R, Müller H, Wiesner T, Jackett LA, Scholz SL, et al. Activating cysteinyl leukotriene receptor 2 (CYSLTR2) mutations in blue nevi. Mod Pathol. 2017;30:350–6. [PubMed: 27934878]
10. Küsters-Vandevelde HVN, Klaasen A, Küsters B, Groenen PJTA, Van Engen-Van Grunsven IACH, Van Dijk MRCF, et al. Activating mutations of the GNAQ gene: A frequent event in primary melanocytic neoplasms of the central nervous system. Acta Neuropathol. 2010;119:317–23. [PubMed: 19936769]
11. Shirley MD, Tang H, Gallione CJ, Baugher JD, Frelin LP, Cohen B, et al. Sturge–Weber Syndrome and Port-Wine Stains Caused by Somatic Mutation in *GNAQ*. N Engl J Med [Internet]. 2013;368:1971–9. Available from: 10.1056/NEJMoa1213507
12. Sheng X, Kong Y, Li Y, Zhang Q, Si L, Cui C, et al. GNAQ and GNA11 mutations occur in 9.5% of mucosal melanoma and are associated with poor prognosis. Eur J Cancer. 2016;65:156–63. [PubMed: 27498141]
13. Küsters-Vandevelde HVN, van Engen- van Grunsven IACH, Coupland SE, Lake SL, Rijntjes J, Pfundt R, et al. Mutations in G Protein Encoding Genes and Chromosomal Alterations in Primary Leptomeningeal Melanocytic Neoplasms. Pathol Oncol Res. 2015;21:439–47. [PubMed: 25315378]
14. Gill RM, Buelow B, Mather C, Joseph NM, Alves V, Brunt EM, et al. Hepatic small vessel neoplasm, a rare infiltrative vascular neoplasm of uncertain malignant potential. Hum Pathol. 2016;54:143–51. [PubMed: 27090685]
15. Joseph NM, Brunt EM, Marginean C, Nalbantoglu Ilk, Snover DC, Thung SN, et al. Frequent GNAQ and GNA14 mutations in hepatic small vessel neoplasm. Am J Surg Pathol. 2018;42:1201–7. [PubMed: 29975248]

16. Zuidervaart W, Van Nieuwpoort F, Stark M, Dijkman R, Packer L, Borgstein AM, et al. Activation of the MAPK pathway is a common event in uveal melanomas although it rarely occurs through mutation of BRAF or RAS. Br J Cancer. 2005;
17. Carvajal RD, Piperno-Neumann S, Kapiteijn E, Chapman PB, Frank S, Joshua AM, et al. Selumetinib in combination with dacarbazine in patients with metastatic uveal melanoma: A Phase III, Multicenter, Randomized Trial (SUMIT). J Clin Oncol. 2018;36:1232–9. [PubMed: 29528792]
18. Ambrosini G, Pratilas CA, Qin L-X, Tadi M, Surriga O, Carvajal RD, et al. Identification of unique MEK-dependent genes in GNAQ mutant uveal melanoma involved in cell growth, tumor cell invasion, and MEK resistance. Clin Cancer Res. AACR; 2012;18:3552–61. [PubMed: 22550165]
19. Moore AR, Ran L, Guan Y, Sher JJ, Zhang JQ, Hwang C, et al. Novel GNA11 Q209L mouse model reveals RasGRP3 as an essential signaling node in uveal melanoma. Cell Rep [Internet]. 2018;22:2455–68. Available from: http://www.cell.com/cell-reports/abstract/S2211-1247(18)30145-1
20. Chen X, Wu Q, Depeille P, Chen P, Thornton S, Kalirai H, et al. RasGRP3 Mediates MAPK Pathway Activation in GNAQ Mutant Uveal Melanoma. Cancer Cell. 2017;
21. Luke JJ, Triozzi PL, McKenna KC, Van Meir EG, Gershenwald JE, Bastian BC, et al. Biology of advanced uveal melanoma and next steps for clinical therapeutics. Pigment Cell Melanoma Res. 2015;
22. Chen X, Wu Q, Tan L, Porter D, Jager MJ, Emery C, et al. Combined PKC and MEK inhibition in uveal melanoma with GNAQ and GNA11 mutations. Oncogene. 2014;33:4724–34. [PubMed: 24141786]
23. Moore AR, Rosenberg SC, McCormick F, Malek S. RAS-targeted therapies: is the undruggable drugged? Nat Rev Drug Discov [Internet]. Springer US; 2020;1–20. Available from: http://www.nature.com/articles/s41573-020-0068-6
24. Lito P, Solomon M, Li L-S, Hansen R, Rosen N. Allele-specific inhibitors inactivate mutant KRAS G12C by a trapping mechanism. Science (80-). 2016;351.
25. Patricelli MP, Janes MR, Li LS, Hansen R, Peters U, Kessler L V., et al. Selective inhibition of oncogenic KRAS output with small molecules targeting the inactive state. Cancer Discov. 2016;6:316–29. [PubMed: 26739882]
26. Janes MR, Zhang J, Li LS, Hansen R, Peters U, Guo X, et al. Targeting KRAS Mutant Cancers with a Covalent G12C-Specific Inhibitor. Cell. 2018;172:578–589.e17. [PubMed: 29373830]
27. Takasaki J, Saito T, Taniguchi M, Kawasaki T, Moritani Y, Hayashi K, et al. A Novel Gaq/11-selective Inhibitor. J Biol Chem. 2004;279.
28. Taniguchi M, Suzumura KI, Nagai K, Kawasaki T, Saito T, Takasaki J, et al. Structure of YM-254890, a novel Gq/11inhibitor from Chromobacterium sp. QS3666. Tetrahedron. 2003;59:4533–8.
29. Nishimura A, Kitano K, Takasaki J, Taniguchi M, Mizuno N, Tago K, et al. Structural basis for the specific inhibition of heterotrimeric Gq protein by a small molecule. Proc Natl Acad Sci. 2010;
30. Uemura T, Kawasaki T, Taniguchi M, Moritani Y, Hayashi K, Saito T, et al. Biological properties of a specific Gαq/11inhibitor, YM-254890, on platelet functions and thrombus formation under high-shear stress. Br J Pharmacol. 2006;148:61–9. [PubMed: 16520742]
31. Roszko KL, Bi R, Gorvin CM, Bräuner-osborne H, Xiong X, Inoue A, et al. Knockin mouse with mutant G α 11 mimics human inherited hypocalcemia and is rescued by pharmacologic inhibitors. 2017;2:1–15.
32. Uemura T, Takamatsu H, Kawasaki T, Taniguchi M, Yamamoto E, Tomura Y, et al. Effect of YM-254890, a specific Gαq/11 inhibitor, on experimental peripheral arterial disease in rats. Eur J Pharmacol. 2006;536:154–61. [PubMed: 16566917]
33. Graziano MP, Gilman AG. Synthesis in Escherichia coli of GTPase-deficient mutants of G(sα). J Biol Chem. 1989;264:15475–82. [PubMed: 2549065]
34. Onken MD, Makepeace CM, Kaltenbronn KM, Kanai SM, Todd TD, Wang S, et al. Targeting nucleotide exchange to inhibit constitutively active G protein a subunits in cancer cells. Sci Signal. 2018;11.

35. Lapadula D, Farias E, Randolph CE, Purwin TJ, McGrath D, Charpentier TH, et al. Effects of oncogenic Gαq and Gα11 inhibition by FR900359 in uveal melanoma. Mol Cancer Res. AACR; 2019;17:963–73. [PubMed: 30567972]
36. Annala S, Feng X, Shridhar N, Eryilmaz F, Patt J, Yang J, et al. Direct targeting of Gαq and Gα11 oncoproteins in cancer cells. Sci Signal. American Association for the Advancement of Science; 2019;12:eaau5948.
37. Schrage R, Schmitz AL, Gaffal E, Annala S, Kehraus S, Wenzel D, et al. The experimental power of FR900359 to study Gq-regulated biological processes. Nat Commun. 2015;
38. Akama-Garren EH, Joshi NS, Tammela T, Chang GP, Wagner BL, Lee D-Y, et al. A modular assembly platform for rapid generation of DNA constructs. Sci Rep. Nature Publishing Group; 2016;6:16836. [PubMed: 26887506]
39. Boehm JS, Zhao JJ, Yao J, Kim SY, Firestein R, Dunn IF, et al. Integrative Genomic Approaches Identify IKBKE as a Breast Cancer Oncogene. Cell. 2007;129:1065–79. [PubMed: 17574021]
40. Bennett D, Cooper P, Hart I. A line of non-tumorigenic mouse melanocytes, syngeneic with the B16 melanoma and requiring a tumour promoter for growth. 1987;414–8.
41. Di Veroli GY, Fornari C, Wang D, Mollard S, Bramhall JL, Richards FM, et al. Combenefit: an interactive platform for the analysis and visualization of drug combinations. Bioinformatics. Oxford University Press; 2016;32:2866–8. [PubMed: 27153664]
42. Jin C, Fotaki G, Ramachandran M, Nilsson B, Essand M, Yu D. Safe engineering of CAR T cells for adoptive cell therapy of cancer using long-term episomal gene transfer. EMBO Mol Med. John Wiley & Sons, Ltd; 2016;8:702–11. [PubMed: 27189167]
43. Dobin A, Davis CA, Schlesinger F, Drenkow J, Zaleski C, Jha S, et al. STAR: ultrafast universal RNA-seq aligner. Bioinformatics. Oxford University Press; 2013;29:15–21. [PubMed: 23104886]
44. Love MI, Huber W, Anders S. Moderated estimation of fold change and dispersion for RNA-seq data with DESeq2. Genome Biol. 2014;15:1–21.
45. Zehir A, Benayed R, Shah RH, Syed A, Middha S, Kim HR, et al. Mutational landscape of metastatic cancer revealed from prospective clinical sequencing of 10,000 patients. Nat Med. 2017;23:703–13. [PubMed: 28481359]
46. Robertson AG, Shih J, Yau C, Gibb EA, Oba J, Mungall KL, et al. Integrative Analysis Identifies Four Molecular and Clinical Subsets in Uveal Melanoma. Cancer Cell. 2017;32:204–220.e15. [PubMed: 28810145]
47. Furney SJ, Pedersen M, Gentien D, Dumont AG, Rapinat A, Desjardins L, et al. SF3B1 mutations are associated with alternative splicing in uveal melanoma. Cancer Discov. 2013;3:1122–9. [PubMed: 23861464]
48. Martin M, Maßhöfer L, Temming P, Rahmann S, Metz C, Bornfeld N, et al. Exome sequencing identifies recurrent somatic mutations in EIF1AX and SF3B1 in uveal melanoma with disomy 3. Nat Genet [Internet]. Nature Publishing Group; 2013;45:933–6. Available from: 10.1038/ng.2674
49. Johnson CP, Kim IK, Esmaeli B, Amin-Mansour A, Treacy DJ, Carter SL, et al. Systematic genomic and translational efficiency studies of uveal melanoma. PLoS One. 2017;12:1–17.
50. Taylor VG, Bommarito PA, Tesmer JJG. Structure of the regulator of G protein signaling 8 (RGS8)-Gαq complex: Molecular basis for Gα selectivity. J Biol Chem. 2016;291:5138–45. [PubMed: 26755720]
51. Akbani R, Akdemir KC, Aksoy BA, Albert M, Ally A, Amin SB, et al. Genomic Classification of Cutaneous Melanoma. Cell. 2015;161:1681–96. [PubMed: 26091043]
52. Huang JLY, Urtatiz O, Van Raamsdonk CD. Oncogenic G protein GNAQ induces uveal melanoma and intravasation in mice. Cancer Res. 2015;
53. Griewank KG, Yu X, Khalili J, Sozen MM, Stempke-Hale K, Bernatchez C, et al. Genetic and molecular characterization of uveal melanoma cell lines. Pigment Cell Melanoma Res. 2012;
54. Pratilas CA, Taylor BS, Ye Q, Viale A, Sander C, Solit DB, et al. V600EBRAF is associated with disabled feedback inhibition of RAF-MEK signaling and elevated transcriptional output of the pathway. Proc Natl Acad Sci U S A. 2009;106:4519–24. [PubMed: 19251651]
55. Lito P, Saborowski A, Yue J, Solomon M, Joseph E, Gadal S, et al. Disruption of CRAF-Mediated MEK activation is required for effective mek inhibition in KRAS mutant tumors. Cancer Cell [Internet]. Elsevier Inc.; 2014;25:697–710. Available from: 10.1016/j.ccr.2014.03.011

56. McCormick F. Targeting KRAS Directly. Annu Rev Cancer Biol. 2018;2:81–90.

57. Taniguchi M, Suzumura KI, Nagai K, Kawasaki T, Takasaki J, Sekiguchi M, et al. YM-254890 analogues, novel cyclic depsipeptides with Gαq/11inhibitory activity from Chromobacterium sp. QS3666. Bioorganic Med Chem. 2004;12:3125–33.

58. Xiong X-F, Zhang H, Underwood CR, Harpsøe K, Gardella TJ, Wöldike MF, et al. Total synthesis and structure–activity relationship studies of a series of selective G protein inhibitors. Nat Chem [Internet]. Nature Publishing Group; 2016;8:1035–41. Available from: 10.1038/nchem.2577

59. Kamato D, Mitra P, Davis F, Osman N, Chaplin R, Cabot PJ, et al. Gaq proteins: molecular pharmacology and therapeutic potential. Cell Mol Life Sci [Internet]. Springer International Publishing; 2017;74:1379–90. Available from: 10.1007/s00018-016-2405-9

60. Zhang H, Xiong X-F, Boesgaard MW, Underwood CR, Bräuner-Osborne H, Strømgaard K. Structure-Activity Relationship Studies of the Cyclic Depsipeptide Natural Product YM-254890, Targeting the G_q Protein. ChemMedChem [Internet]. 2017;12:830–4. Available from: 10.1002/cmdc.201700155

Translational Relevance

All uveal melanoma and a fraction of other melanoma subtypes are driven by activation of the $G\alpha_q$ pathway. There are no clinically efficacious systemic therapies for these melanomas. Recent work has shown promising preclinical activity of natural compounds that directly inhibit $G\alpha_q$, but their clinical use is potentially limited by narrow therapeutic window from inhibition of normal $G\alpha_q$. Here, we describe synergistic efficacy of the $G\alpha_q$ inhibitor YM-254890 and clinically used MEK inhibitors in engineered models driven by distinct mutations in $G\alpha_q$ and in *CYSLTR2* as well as in multiple human uveal melanoma cell lines. Our work suggests that the combination leads to sustained inhibition of the MAPK pathway and synergistic growth inhibition. Combination treatment *in vivo* led to increased MAPK pathway inhibition and tumor shrinkage. Together, this work nominates combination of $G\alpha_q$ and MEK inhibition as a strategy for targeting $G\alpha_q$ driven melanoma clinically.

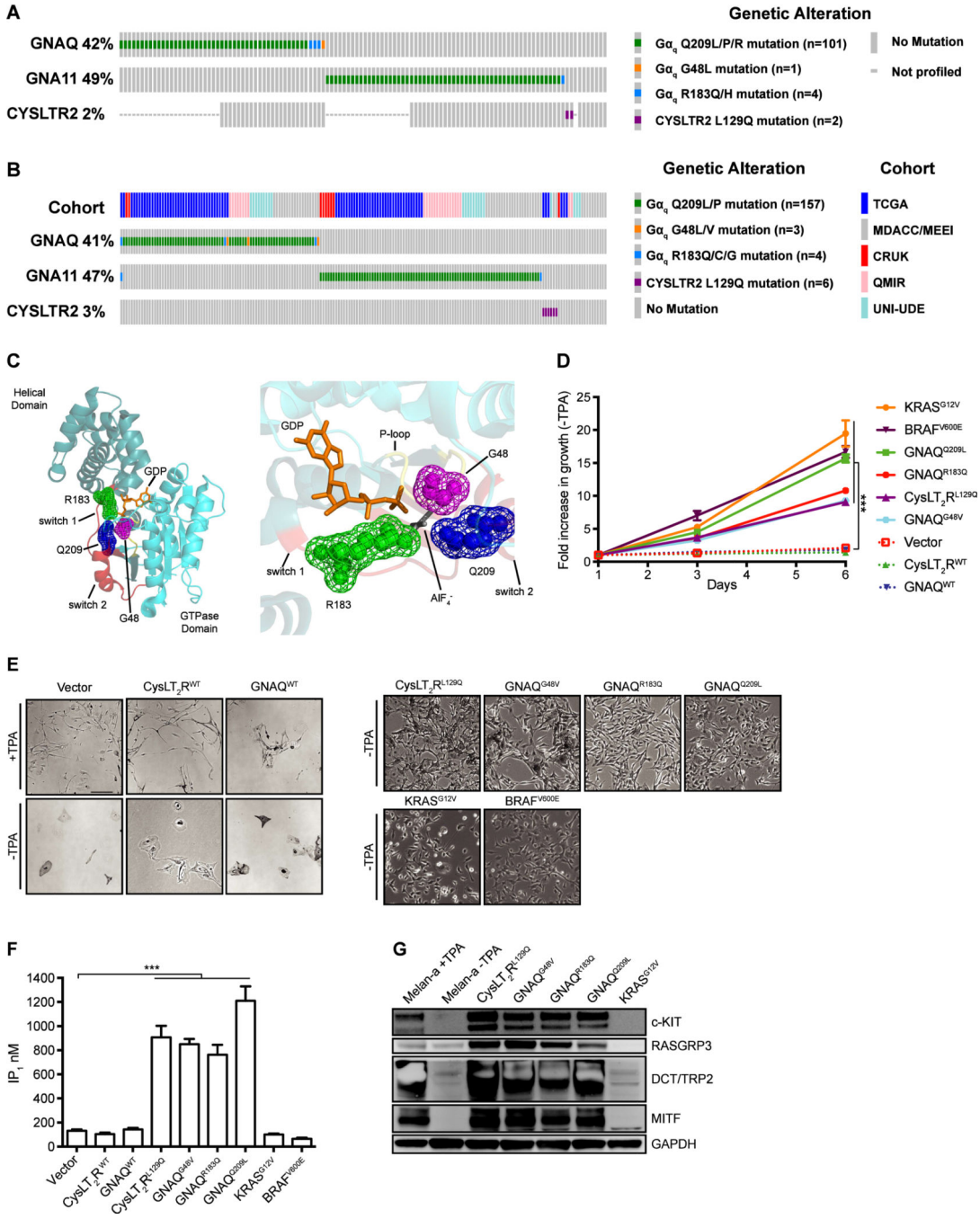

Figure 1.

$G\alpha_q$ mutations occur at three hotspot residues that are known to affect the guanine-nucleotide binding pocket. **(A)** Oncoprint of $G\alpha_q$ pathway mutations in 116 UVM patients who have undergone MSK-IMPACT testing. **(B)** Oncoprint of $G\alpha_q$ pathway mutations in 188 UVM patients from five published cohorts including TCGA (46), Cancer Research UK (CRUK) (47), QIMR Berghofer Medical Research Institute (8), University of Duisburg-Essen (UNI-UDE) (48) and MD Anderson Cancer Center/Massachusetts Eye and Ear Infirmary (MDACC/MEEI) (49). **(C)** 3D cartoon structure of GNAQ (left) highlighting

Gly48 (magenta) of the P-loop (yellow), Arg183 (green) of Switch 1 (red), and Gln209 (blue) of Switch 2 (red). GDP (orange) and AlF_4^- (grey) are both shown as sticks and the three residues are shown as mesh spheres. Close up view of GTP binding pocket (right). Structure from Protein Data Bank Entry 5DO9 (50). **(D)** Growth assay for melan-a cells in the absence of TPA for six days. Growth was assayed by Celltiter-Glo 2.0 at D1, D3, and D6. Fold increase in luminescence is shown relative to D1 cell number. **(E)** Phase contrast images of engineered melan-a cells after TPA withdrawal for 2 weeks (scale bar 100μm). **(F)** Basal level of IP_1 accumulation in melan-a cells. Vector and WT controls are cultured with TPA whereas the remaining samples were cultured without TPA. **(G)** Western blot of melanocyte lineage markers (MITF, TRP2/DCT, c-KIT, and RASGRP3) upon TPA withdrawal for 2 weeks. For all cases (mean ± SEM, n = 3), $P < 0.0005$; ***, vector compared against each condition.

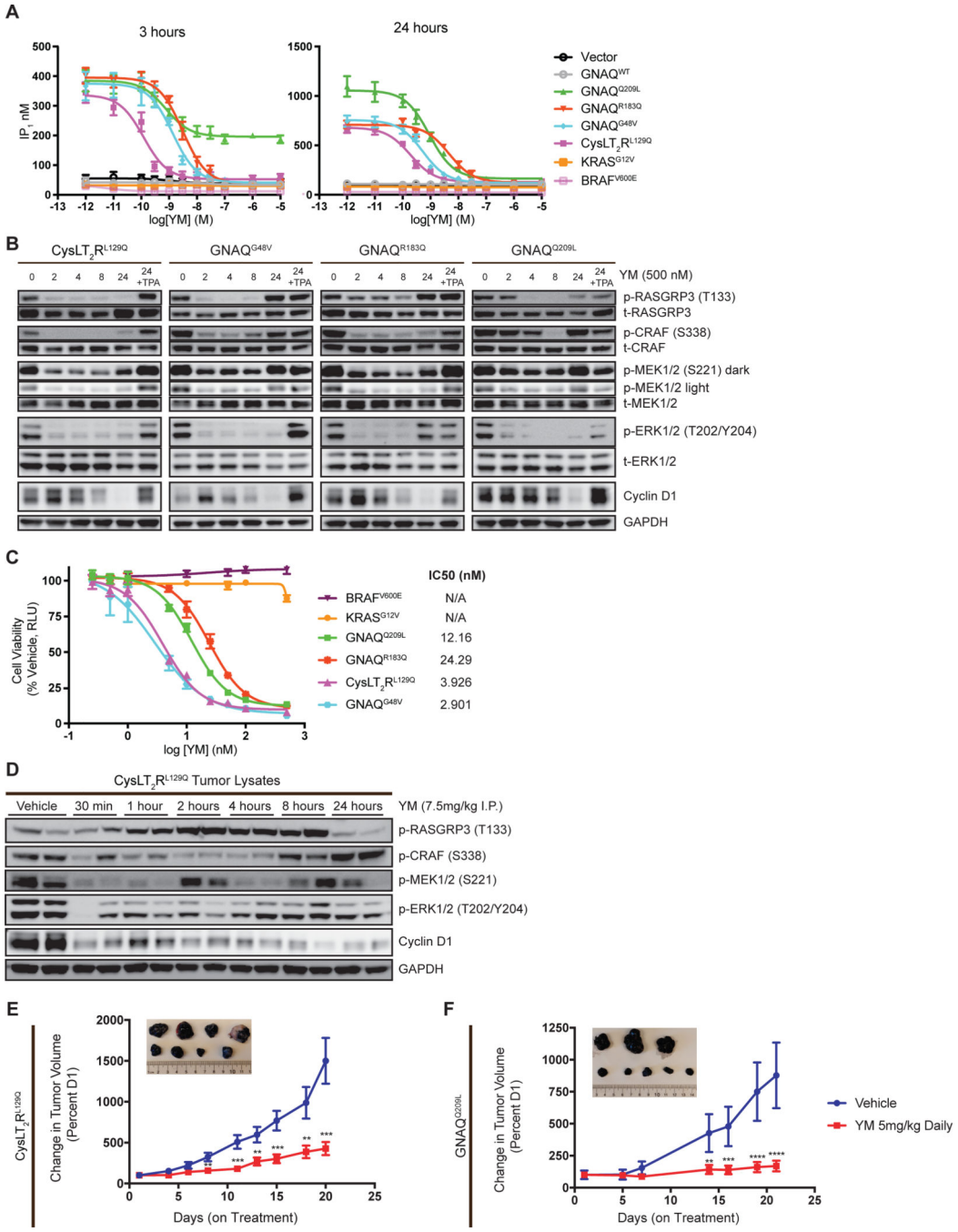

Figure 2.

YM-254890 inhibits mutation dependent melan-a cell tumor growth and signaling. **(A)** IP_1 accumulation assays in mutation dependent melan-a cells. Cells were treated with increasing concentrations of YM for 3 hours (left) and 24 hours (right). Data are expressed as IP_1 concentration (nM) (mean ± SEM, n = 3). **(B)** Western blot analysis of MAPK signaling in melan-a cells treated with 500nM YM at 0, 2, 4, 8, and 24 hours; the last sample for each cell line was also treated with TPA for 24 hours showing rescue of the pathway. **(C)** Dose response of melan-a cells treated with YM for 5 days at increasing dose and readout by

CellTiter Glo 2.0. Data are expressed as the percentage RLU relative to that observed with vehicle. (mean ± SEM, n = 3). **(D)** Western blot of lysates from $CysLT_2R^{L129Q}$ melan-a tumors harvested at the indicated time after a single dose YM (7.5mg/kg). **(E)** Percent tumor volume of $CysLT_2R^{L129Q}$ and **(F)** $GNAQ^{Q209L}$ melan-a allografts treated with vehicle or YM daily. Pictures of representative tumors are vehicle (top) and YM treated (bottom) at the end of treatment (mean ± SEM, n = 6–10). For all cases $P < 0.005$; **, $P < 0.0005$; ***, $P < 0.0001$; ****.

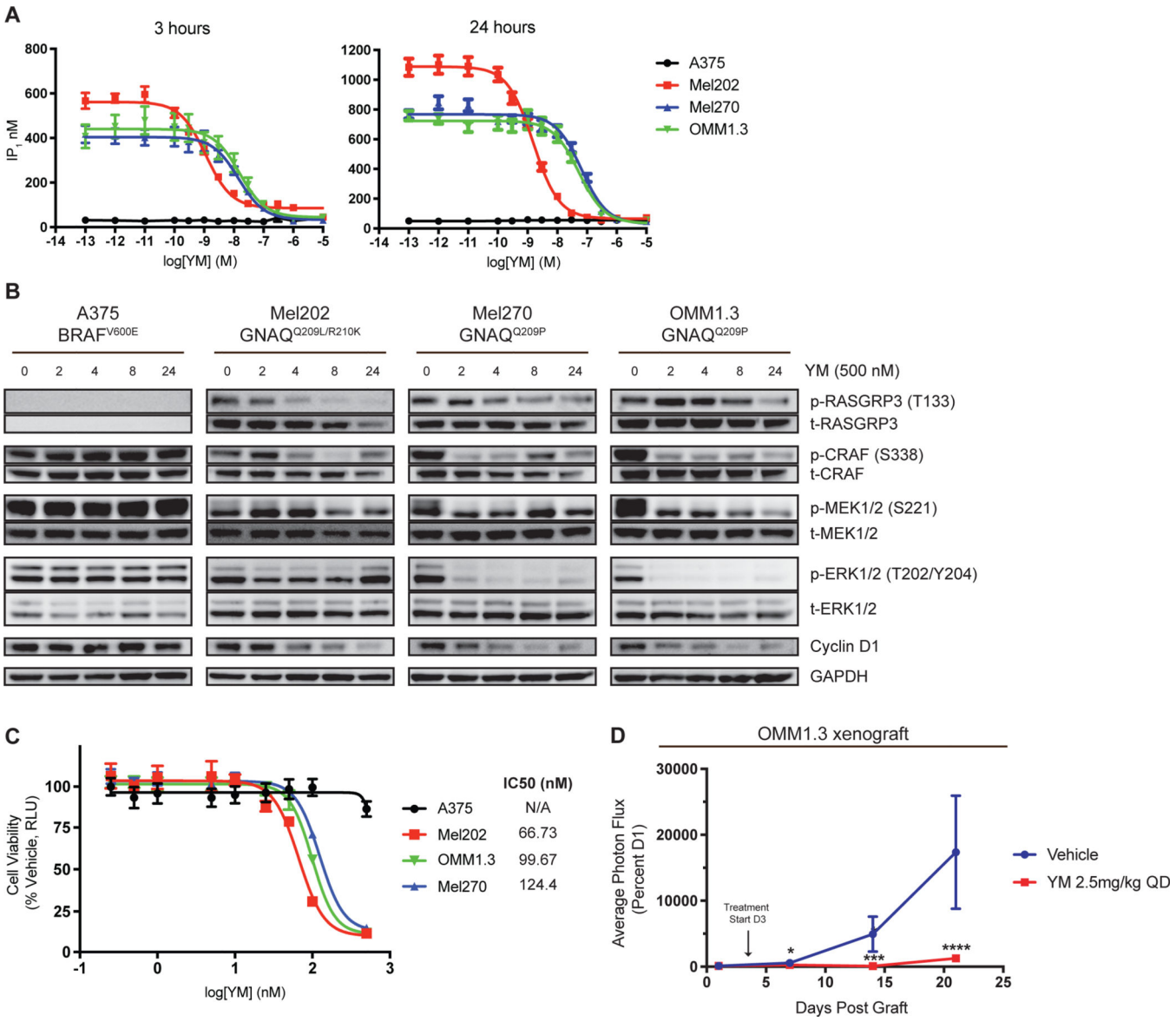

Figure 3.

YM-254890 inhibits human UVM cell signaling and tumor growth. **(A)** IP_1 accumulation assay in UVM cells and A375 cells (cutaneous $BRAF^{V600E}$). Cells were treated with increasing concentrations of YM for 3 hours (left) and 24 hours (right). Data are expressed as IP_1 concentration (nM) (mean ± SEM, n = 3) **(B)** Western blot analysis of indicated proteins in UVM cells and A375 cells treated with 500nM YM at 0, 2, 4, 8, and 24 hours. **(C)** Dose response of UVM and A375 cells treated with YM for 5 days at increasing dose and readout by CellTiter Glo 2.0. Data are expressed as the percentage RLU relative to that observed with vehicle. (mean ± SEM, n = 3). **(D)** Percent photon flux of OMM1.3 xenografts treated with vehicle or YM (2.5mg/kg) for 21 days (mean ± SEM, n = 10). Cells were transduced with pBMN for luciferase expression. Arrow indicates start of treatment at day 3. $P < 0.05$; *, $P < 0.0005$; ***, $P < 0.0001$, ****.

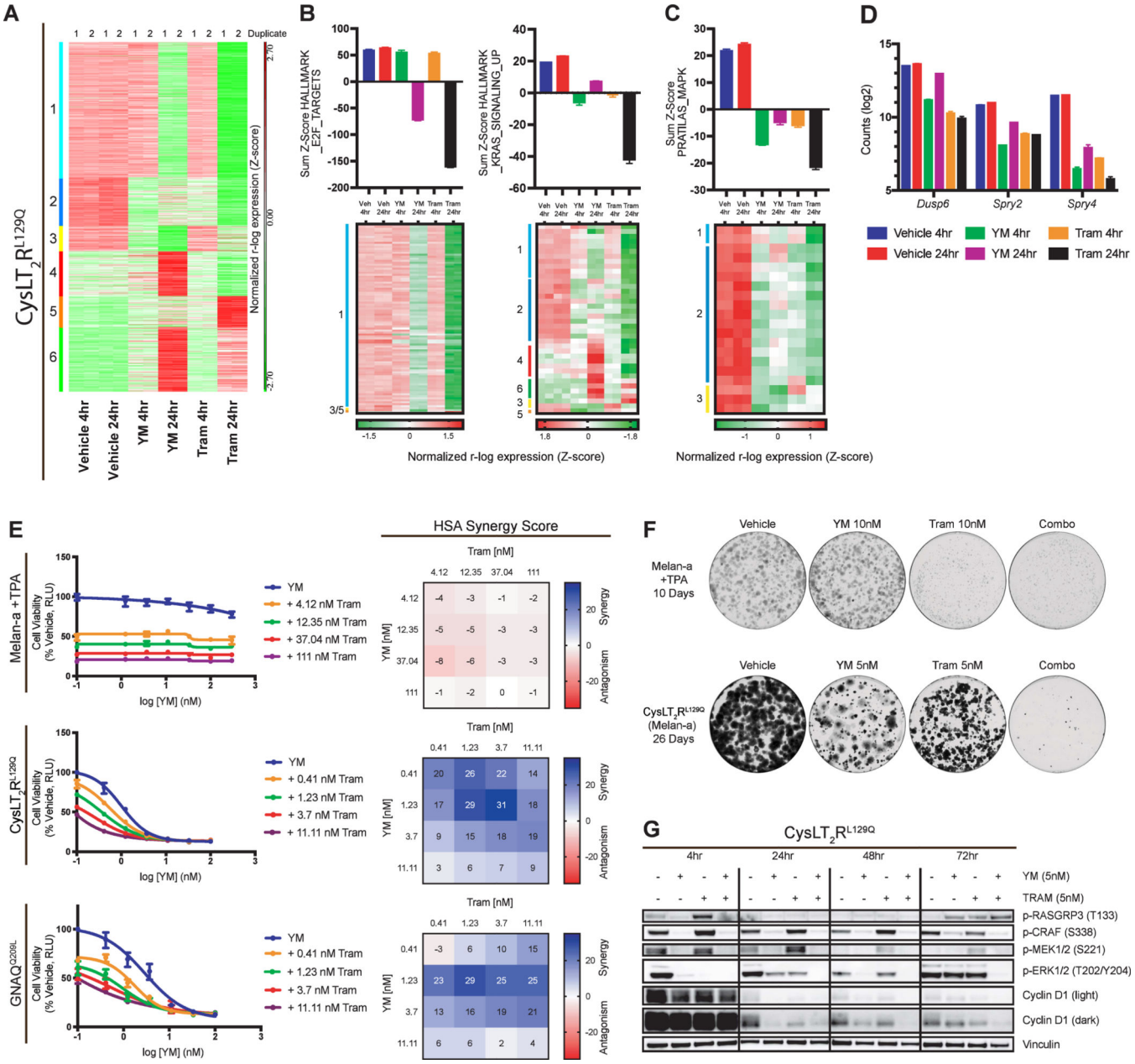

Figure 4.

Transcriptomics implicates synergistic action between $G\alpha_q$ inhibition and MEK inhibition in melan-a cells. **(A)** Heatmap of RNA-seq gene expression from $CysLT_2R^{L129Q}$ melan-a cells treated with vehicle, YM (100nM), or trametinib (100nM) for 4 or 24 hours (duplicates shown). Data was r-log transformed, Z-scored, and then k-means clustered. Clusters are labeled 1–6 and color coordinated (left). **(B)** Sum Z-scores of E2F_Targets, KRAS_SIGNALING_UP, and **(C)** Pratilas_MAPK are shown (top) with heatmaps (bottom) showing expression of individual signature genes (mean ± SEM, n = 2). **(D)** RNA-seq based expression (log_2 count) of *Dusp6*, *Spry2*, and *Spry4* (mean ± SEM, n = 2). **(E)** Viability curves for melan-a cell lines treated with increasing doses of YM in combination with four

doses of trametinib (left) and corresponding HSA synergy diagrams (right) (mean ± SEM, n = 3). **(F)** Growth assays for parental melan-a cells (+TPA) and $CysLT_2R^{L129Q}$ melan-a cells (-TPA) in the presence of vehicle, YM, trametinib, or Combo for 10 or 26 days, respectively. **(G)** Western blot analysis of indicated proteins in $CysLT_2R^{L129Q}$ melan-a cells. Cells were treated with vehicle, YM, trametinib, or Combo for 4, 24, 48, and 72 hours.

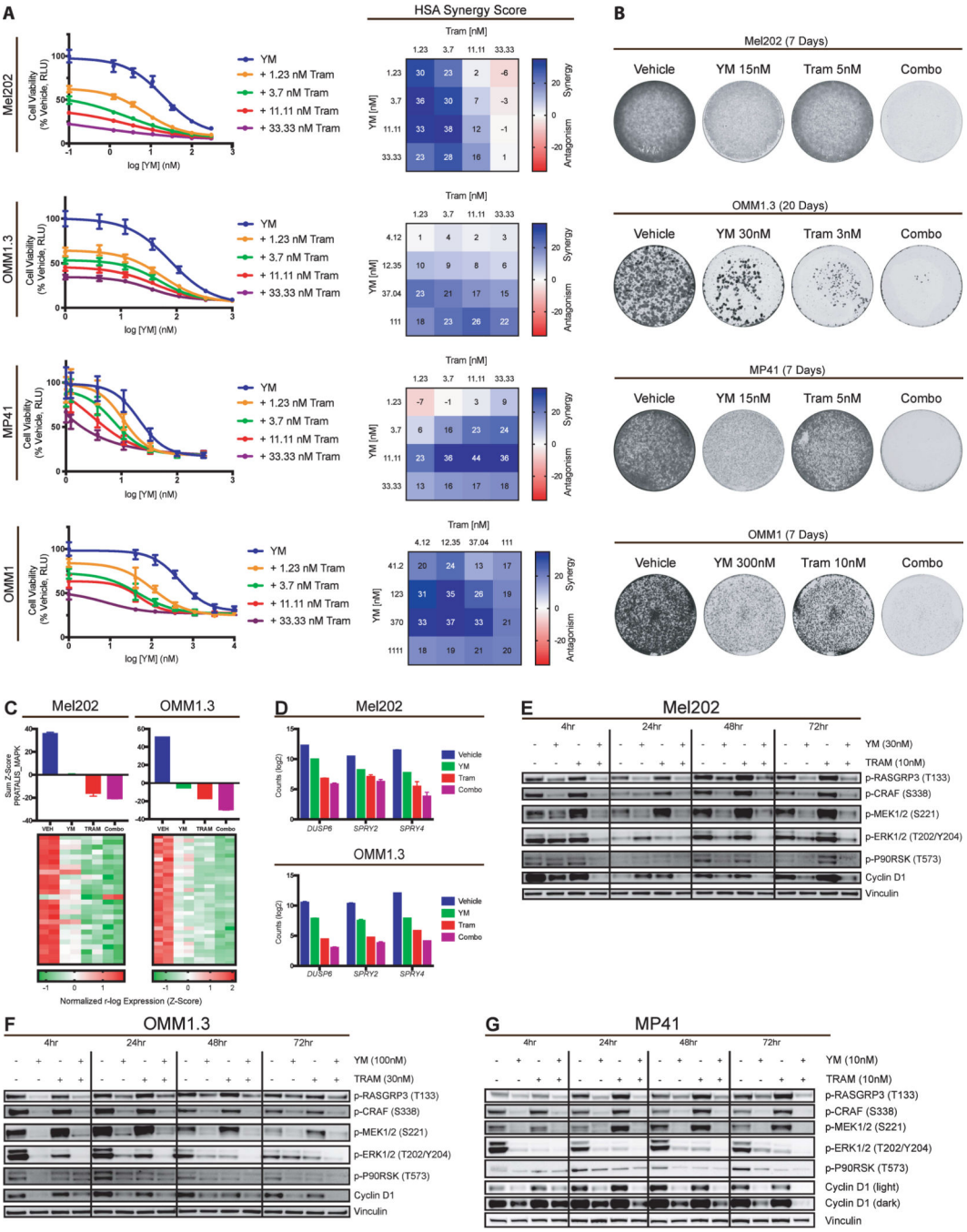

Figure 5.

YM-254890 and MEKi lead to sustained MAPK inhibition in UVM cells. **(A)** Viability curves for four UVM cell lines treated with increasing doses of YM in combination with four doses of trametinib (left) and corresponding HSA synergy diagrams (right). (mean ± SEM, n = 3). **(B)** Growth assays of Mel202, OMM1.3, MP41, and OMM1 cells treated with vehicle, YM, trametinib, or Combo. **(C)** Mel202 and OMM1.3 sum Z scores of Pratilas_MAPK are shown (top) with heatmaps (bottom) showing expression of individual signature genes (mean ± SEM, n = 2). **(D)** Expression counts (log_2) of *DUSP6*, *SPRY2*, and

SPRY4 from RNA-seq data for Mel202 and OMM1.3 cells (mean ± SEM, n = 2). **(E)** Western blot analysis of indicated proteins in Mel202, **(F)** OMM1.3, and **(G)** MP41 cells. Cells were treated with vehicle, YM, trametinib, or Combo for 4, 24, 48, and 72 hours.

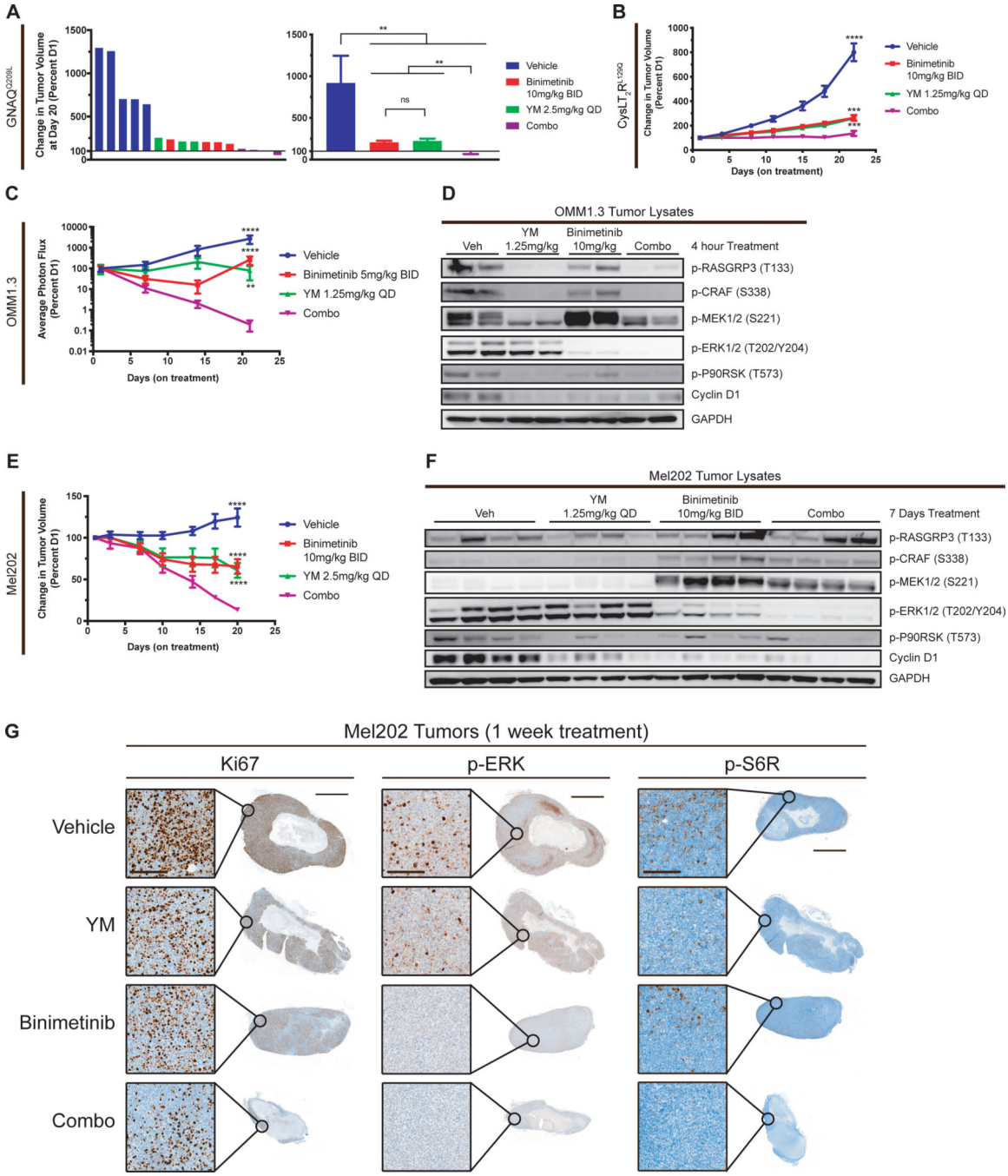

Figure 6.

Combination of YM-254890 and binimetinib *in vivo* inhibits tumor growth and signaling. **(A)** Percent tumor volume of individual tumors (left) and averaged (right) of $GNAQ^{Q209L}$ melan-a allografts treated with vehicle, YM, binimetinib, or Combo for 20 days (mean ± SEM). Origin (Y=100) represents no change in tumor volume. **(B)** Percent tumor volume of $CysLT_2R^{L129Q}$ melan-a allografts treated with vehicle, YM, binimetinib, or Combo for 22 days (mean ± SEM, n = 10). **(C)** Percent photon flux of OMM1.3 xenografts treated with vehicle, YM, binimetinib, or Combo daily for 21 days (mean ± SEM, n = 4–10). Cells were

transduced with pBMN for luciferase expression. **(D)** Western blot of OMM1.3 tumors treated for 4 hours with vehicle, YM, binimetinib, and Combo. **(E)** Percent tumor volume of Mel202 xenografts treated with vehicle, YM, binimetinib, or Combo for 20 days (mean ± SEM, n = 4–6). **(F)** Western blot of Mel202 tumors treated for 1 week with vehicle, YM, binimetinib, and Combo. **(G)** Immunohistochemistry of Mel202 tumors from (Figure 6F) for Ki67, p-ERK, and p-S6R. Scale bar, 50μm for insert (left) and 2mm for whole tumor (right). For all cases $P > .05$; ns, $P < 0.005$; **, $P < 0.0005$; ***, $P < 0.0001$, ****.